Bull. Astr. Soc. India (1999) **27**, 583-600

Infrared diagnostics for compact H II Regions - II

Bhaswati Mookerjea[1] and S. K. Ghosh[2]

Tata Institute of Fundamental Research, Homi Bhabha Road, Mumbai 400005, India

Received 25 April 1999; accepted 16 July 1999.

Abstract. Compact H II regions have been realistically modelled to identify the wavelength regime and type of observables, which are crucial for understanding the physical conditions of the same. Spherically symmetric interstellar clouds of dust and gas, with an embedded exciting star, have been considered. Radiation transfer through these clouds have been carried out to predict : infrared photometric colours, angular sizes, luminosities of infrared fine structure lines from heavier elements in gas phase and radio continuum emission.

The study has been divided into two categories : either all the model clouds are constrained to have (i) a fixed total mass; or (ii) a fixed physical size. Detailed study of the first category has been presented in Mookerjea & Ghosh (1999a, Paper I). Here we present the second category of models, where (a) the study has been extended by including high resolution spectroscopic diagnostics; and (b) a wider range of radial density distribution laws have been considered.

Three types of embedded stars, viz., ZAMS O4, O7 and B0.5 have been considered and a wide range of optical depth has been covered. All relevant model predictions have been quantified in terms of observables with different instruments onboard the Infrared Space Observatory (ISO) for direct comparability.

The present study has quantified the importance of high resolution mid and far infrared spectroscopy in determining the elemental abundances, embedded stellar type, temperature & density distribution and geometrical details of compact H II regions. The diagnostic value of infrared colours and angular size, show trends similar to those presented in Paper I.

Key words : compact H II regions - radiative transfer - infrared colours - nebular lines

[1]bhaswati@tifr.res.in, [2]swarna@tifr.res.in

1. Introduction

The evolution of the protostellar core to form a high mass star is not observable as clearly as the different developmental stages of a low mass star. However, the sites of formation of high mass star bear good infrared and radio signatures, while the star is embedded in the interstellar material from which it is formed. The compact H II regions are formed as a result of this interplay between the high luminosity of these stars and the gas surrounding them. Hence, the compact H II regions can act as excellent probes to understand the formation of mid to high mass stars. Study of compact H II regions is made easier by the predominantly spherical geometry and the availability of observational data over a large range (infrared-sub-mm-radio) of wavelengths. With this in mind a programme has been undertaken to model the compact H II regions self-consistently. The first part of the programme (Mookerjea & Ghosh 1999a, hereafter Paper I) deals with compact H II regions for which the total mass estimate exists and the physical sizes etc. are determined by the mass and other physical conditions. The second part, as presented here, deals with H II regions for which the outer physical sizes are known, with no other constraints.

The present study consists of two modelling schemes. The first (I) scheme is identical to that described in Paper I, but for the fact that constraint on physical size replaces that on the total mass. The second (II) is a completely independent scheme, with more detailed radiation transfer through the interstellar gas component. Each model consists of a spherical cloud of dust and gas, illuminated by an exciting star at the centre and the interstellar radiation field (ISRF) at the outer boundary. All the models are assumed to have the same outer physical dimension. The following parameters are varied :-the type of ZAMS star acting as the central exciting source, the radial density distribution (of the dust and the gas) and the total dust optical depth. The effects of these variations on the continuum (from the dust and the gas), as well as on the infrared fine structure line emission (from several heavy elements in gas phase) are studied. As in Paper I, the model predictions from the scheme I include dust continuum emission from UV to millimetre and the radio continuum emission from the gas component at 5 GHz. The scheme II predicts the absolute and relative strengths of several atomic / nebular lines. The predictions from scheme I are presented in terms of (i) colours in various ISOPHOT (the photometer onboard Infrared Space Observatory, ISO) filters; (ii) radial profiles / half sizes in various ISOCAM (the imaging camera onboard ISO) bands ; & (iii) ratio of far infrared (FIR; 60 μm) to radio (5 GHz) flux densities; as a function of radial optical depth (defined at the wavelength of 100 μm, hereafter τ_{100}). The predictions from scheme II are expressed in terms of quantities as would be observed by the Long Wavelength Spectrometer (LWS; Clegg et al., 1996) and the Short Wavelength Spectrometer (SWS; de Graauw et al., 1996) onboard the ISO.

2. Modelling the compact H II regions

In the present study, the compact H II regions have been modelled, using two independent schemes. The first scheme, which is identical to the method described in Paper I, uses a modified version of the radiative transfer code CSDUST3 (Egan et al., 1988). However, unlike Paper I, in this study different models correspond to different total masses, determined by the outer physical size (invariant for all models) and the radial optical depth at 100 μm (τ_{100}). Also,

in this study, the r^{-2} density distribution has been explored in addition to the r^0 and r^{-1} cases.

The second modelling scheme, capable of treating the gas component (along with absorption effects of dust) uses the code CLOUDY(Ferland, 1996), supplemented by an additional software scheme developed by us. CLOUDY self-consistently deals with almost all physical processes (radiative-collisional equilibrium) in and around a photoionized nebula. It simultaneously looks for statistical and thermal equilibrium by solving the equation balancing ionization-neutralization processes and heating-cooling processes. The supplementary scheme to CLOUDY improves the modelling by (i) emulating the exact structure of the compact H II region and (ii) including the absorption effects of the dust (present within the line emitting zone as well as along the line of sight to that zone). For self consistency between the two radiation transfer schemes I & II, the entire cloud is divided into two spherical shells, the inner one being made of only gas (since grains get destroyed very close to the stars) and the outer one with gas and dust. Details of this supplementary scheme are presented in Mookerjea & Ghosh (1999b) and Mookerjea et al. (1999).

The emission line transfer in CLOUDY is treated using the escape probability method (Elitzur 1982). This method is exact if the physical conditions do not vary drastically across the line emitting region. The applicability of this method to the present study of compact H II regions can be justified on the following grounds : (i) the region emitting a particular line is physically very small compared to the extent of the cloud; (ii) the thermal line widths ($\leq$ 1km/ sec) are much smaller than the typical velocity gradient observed in H II regions (Keto 1990; Olmi et al. 1995) due to expansion and rotation.

Table 1. Parameters for O4 type exciting star (R_{min} = 2.30 × 10^{-3} pc)

τ_{100}	r^0		r^{-1}		r^{-2}	
	R_{HII}	$n_d(R_{min})$	R_{HII}	$n_d(R_{min})$	R_{HII}	$n_d(R_{min})$
	(10^{-2}pc)	(10^{-7}cm^{-3})	(10^{-3}pc)	(10^{-4}cm^{-3})	(10^{-3}pc)	(10^{-4}cm^{-3})
0.0045	75.5	0.781	181	0.100	2.30	0.679
0.006	59.5	1.042	78.2	0.134	2.30	0.906
0.008	46.8	1.390	37.6	0.178	2.30	1.207
0.012	33.4	2.085	16.3	0.267	2.30	1.811
0.020	21.7	3.474	7.63	0.446	2.30	3.018
0.050	9.99	8.686	3.65	1.115	2.30	7.546
0.075	7.09	13.03	3.09	1.672	1.95	11.32
0.100	5.56	17.37	2.85	2.230	1.50	15.09
0.150	3.96	26.06	2.63	3.345	1.28	22.64
0.200	3.11	34.74	2.53	4.460	1.22	30.18
0.250	2.59	43.43	2.47	5.575	1.19	37.73
0.300	2.23	52.12	2.43	6.690	1.18	45.27
0.340	2.02	59.06	2.40	7.582	1.17	51.31

Table 2. Parameters for O7 type exciting star (R_{min} = 5.80 × 10^{-4} pc).

τ_{100}	r^0		r^{-1}		r^{-2}	
	R_{HII}	$n_d(R_{min})$	R_{HII}	$n_d(R_{min})$	R_{HII}	$n_d(R_{min})$
	(10^{-2}pc)	(10^{-7}cm^{-3})	(10^{-4}pc)	(10^{-4}cm^{-3})	(10^{-4}pc)	(10^{-3}cm^{-3})
0.0045	40.5	0.781	353	0.331	5.80	0.269
0.006	32.3	1.041	162	0.441	5.80	0.359
0.008	25.8	1.389	81.8	0.588	5.80	0.478
0.012	18.8	2.083	37.1	0.882	5.80	0.717
0.020	12.5	3.471	18.0	1.469	5.80	1.195
0.050	5.98	8.679	8.86	3.674	3.44	2.988
0.075	4.30	13.02	7.56	5.510	3.12	4.482
0.100	3.40	17.36	6.98	7.347	3.02	5.976
0.150	2.44	26.04	6.44	11.02	2.95	8.964
0.200	1.92	34.71	6.13	14.69	2.93	11.95
0.250	1.60	43.39	4.81	18.37	2.92	14.94
0.300	1.38	52.07	3.34	22.04	2.91	17.93
0.340	1.24	59.01	2.60	24.98	2.91	20.32

Table 3. Parameters for B0.5 type exciting star (R_{min} = 1.60 × 10^{-4} pc).

τ_{100}	r^0		r^{-1}		r^{-2}	
	R_{HII}	$n_d(R_{min})$	R_{HII}	$n_d(R_{min})$	R_{HII}	$n_d(R_{min})$
	(10^{-3}pc)	(10^{-7}cm^{-3})	(10^{-6}pc)	(10^{-4}cm^{-3})	(10^{-5}pc)	(10^{-3}cm^{-3})
0.0045	89.69	0.781	1595	1.035	10.74	0.974
0.006	73.37	1.041	9544	1.380	9.339	1.299
0.008	59.97	1.388	615.0	1.840	8.702	1.732
0.012	45.07	2.082	374.6	2.760	8.297	2.598
0.020	31.38	3.471	237.1	4.599	8.105	4.329
0.050	16.27	8.677	58.55	11.53	8.017	10.82
0.075	12.13	13.02	26.02	17.25	8.007	16.24
0.100	9.837	17.35	14.64	23.03	8.004	21.65
0.150	7.311	26.03	6.506	34.50	8.002	32.47
0.200	5.917	34.71	3.660	45.99	8.001	43.29
0.250	5.018	43.38	2.342	57.49	8.001	54.12
0.300	4.385	52.06	1.626	68.99	8.000	64.94
0.340	3.997	59.00	1.266	78.19	8.000	73.60

2.1 The Models

The models are constrained by their physical sizes, so that it is easy to compare the predictions with compact H II regions of known sizes and hence of known distance and luminosity. Three types of exciting stars, viz., O4, O7 and B0.5 are considered. For each stellar type, r^0, r^{-1} and r^{-2}, radial density distributions are considered. For each density distribution, 13 models, with τ_{100} ranging from 0.0045 to 0.34 are considered. For every model the inner dust radius (R_{min}) is determined by the density of dust, the stellar luminosity and the dust sublimation temperature. The outer radius is assumed to be 2 pc for every model. For scheme I the gas and the dust composition and also the ISRF at the outer boundary are the same as those in Paper I. For scheme II, the gas component is assumed to have typical H II region abundances (an average of Baldwin et al., 1991, Osterbrock et al.,1992 & Rubin et al., 1991, as computed by Ferland, 1996). Only those elements having abundances (relative to hydrogen) more than 3×10^{-6} are taken into consideration. Thus in scheme II, the gas consists of H, He, C, N, O, Ne, Mg, Si, S and Ar and the dust is composed of silicate and graphite grains in equal quantities. Geometrical details of these models are presented in Tables 1, 2 and 3 for exciting sources corresponding to ZAMS stars of types O4, O7 and B0.5 respectively. The parameters presented in these tables are self-explanatory, and follow the same naming convention, as in Paper I.

3. Results

3. 1 Continuum emission from the dust and the gas

The variations of the slopes of the spectral energy distributions (SED) as a function of τ_{100}, radial density distribution law, type of exciting star etc. are quantified as colours directly observable using the ISOPHOT. Details about the choice of filters and their characteristics (Table 5 in Paper I) have been presented in Paper I. Figures 1-3 represent the variation of colours as a function of τ_{100}, corresponding to a central star of type O4, O7 and B0.5 respectively. In each figure the model predictions corresponding to dust density profiles varying as r^0, r^{-1} and r^{-2} are presented.

A few colour-colour plots, selected on the basis of their diagnostic values are presented in Figures 4-6. While selecting the colours, it has been ensured that there is no filter, which is common to both the axes, so that any correlation seen, can be regarded as genuine.

Figure 7 presents the variation of the ratio of the predicted radio continuum flux density at 5 GHz and the FIR flux density at 60 μm, with the optical depth. The different curves correspond to the different density distributions, as explained in their captions. In this figure, there are two curves corresponding to the r^{-2} distribution, for different assumptions about the inner radius of the gas cloud (details in Section 4.4).

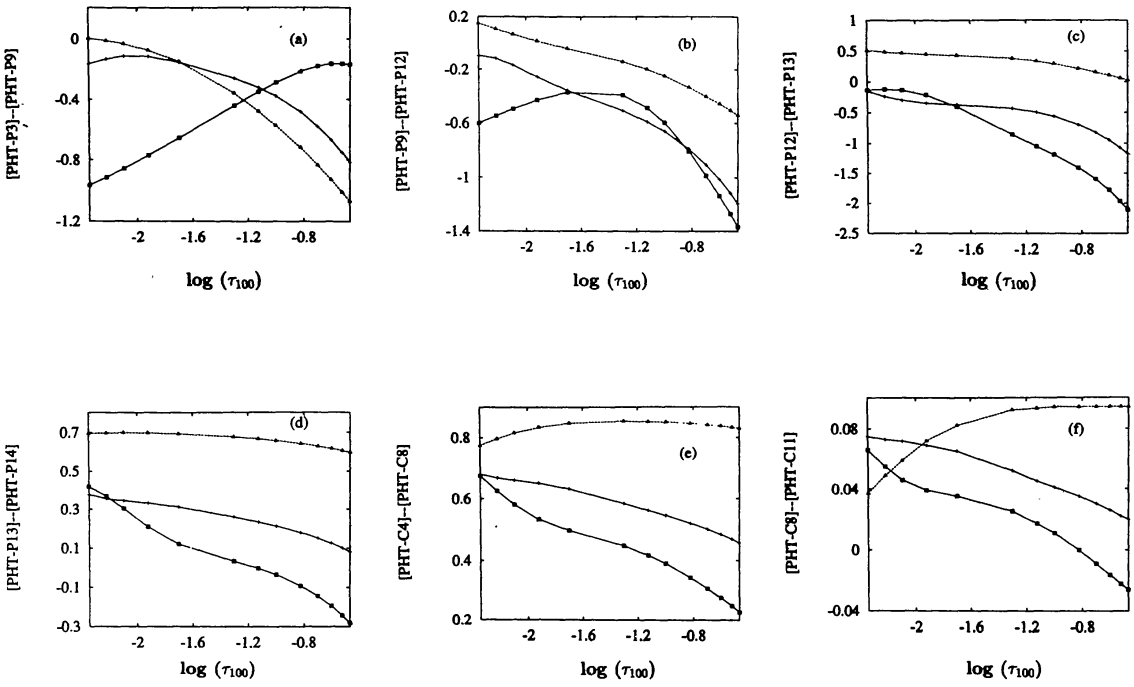

Figure 1. Plots of colours as a function of optical depth τ_{100}, for an exciting star of type O4. The symbols □, + and Δ represent r^0, r^{-1} and r^{-2} density distributions respectively. The ordinates of the plots are : - Colour using PHT-P3 and PHT-P9 filters in (a), PHT-P9 and PHT-P12 filters in (b), PHT-P12 and PHT-P13 filters in (c), PHT-P13 and PHT-P14 filters in (d), PHT-C4 and PHT-C8 filters in (e), PHT-C8 and PHT-C11 filters in (f).

Table 4. Fitted values of the parameter a & b of $\theta_{1/2}(\lambda) = b \times \lambda^a$

Spectral type	r^0		r^{-1}		r^{-2}	
	$\tau_{100} = 0.012$	$\tau_{100} = 0.20$	$\tau_{100} = 0.012$	$\tau_{100} = 0.20$	$\tau_{100} = 0.012$	$\tau_{100} = 0.020$
O4	a = 0.56 b = 15.96	a = 0.31 b = 16.01	a = 0.14 b = 15.92	a = 0.34 b = 15.74	a = 0.15 b = 15.83	a = 0.41 b = 15.66
O7	a = 0.65 b = 15.28	a = 0.46 b = 15.41	a = 0.19 b = 15.31	a = 0.34 b = 15.14	a = 0.15 b = 15.24	a = 0.43 b = 15.06
B0.5	a = 1.02 b = 14.24	a = 0.62 b = 14.77	a = 0.14 b = 14.82	a = 0.33 b = 14.61	a = 0.14 b = 14.70	a = 0.40 b = 14.55

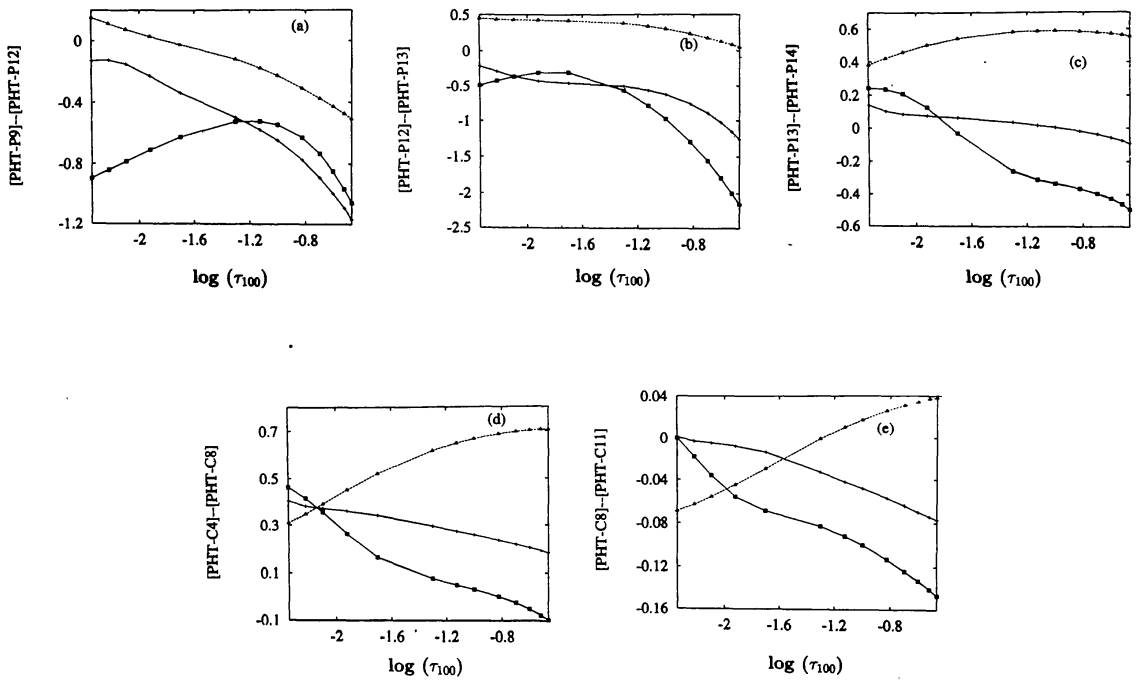

Figure 2. Plots of colours as a function of optical depth τ_{100}, for an exciting star of type O7. The symbols □, + and Δ represent r^0, r^{-1} and r^{-2} density distributions respectively. The ordinates of the plots are : - Colour using PHT-P9 and PHT-P12 filters in (a), PHT-P12 and PHT-P13 filters in (b), PHT-P13 and PHT-P14 filters in (c), PHT-C4 and PHT-C8 filters in (d), PHT-C8 and PHT-C11 filters in (e).

Table 5. List of all the emission lines which have been considered

Element (ionization stage)	λ(μm)	Element (ionization stage)	λ(μm)	Element (ionization stage)	λ(μm)
C II	157.7	S III	33.5	Ne II	12.8
O I	145.6	O IV	25.9	S IV	10.5
N I	121.8	Ne V	24.3	Ar III	8.99
O III	88.4	Ar III	21.8	Ar V	7.91
O I	63.2	S III	18.7	Ne VI	7.66
N III	57.2	Ne III	15.6	Ar II	6.99
O III	51.8	Ne V	14.3	Mg V	5.61
Ne III	36.0	Ar V	13.5	Ar VI	4.53
Si II	34.8	Mg V	13.1	Mg IV	4.49

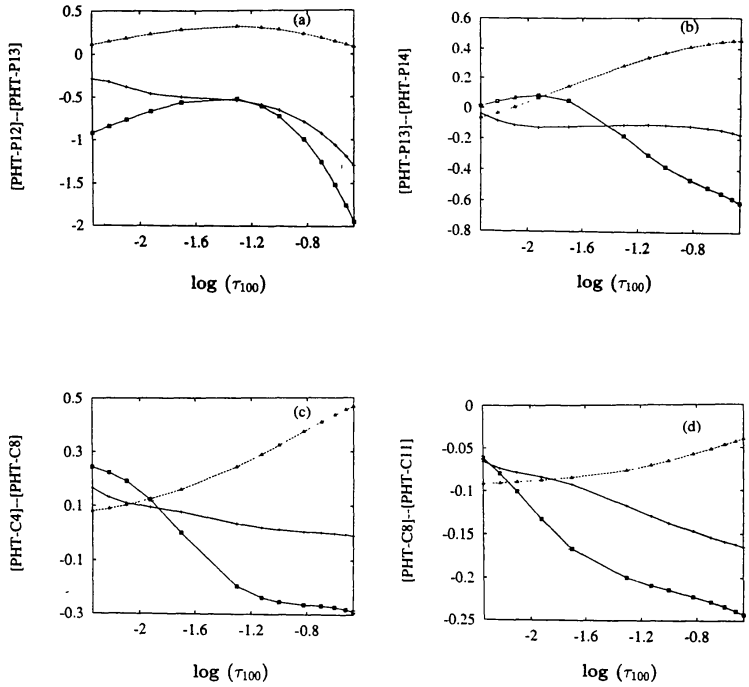

Figure 3. Plots of colours as a function of optical depth τ_{100}, for an exciting star of type B0.5. The symbols □ , + and Δ represent r^0, r^{-1} and r^{-2} density distributions respectively. The ordinates of the plots are : - Colour using PHT-P12 and PHT-P13 filters in (a), PHT-P13 and PHT-P14 filters in (b), PHT-C4 and PHT-C8 filters in (c), PHT-C8 and PHT-C11 filters in (d).

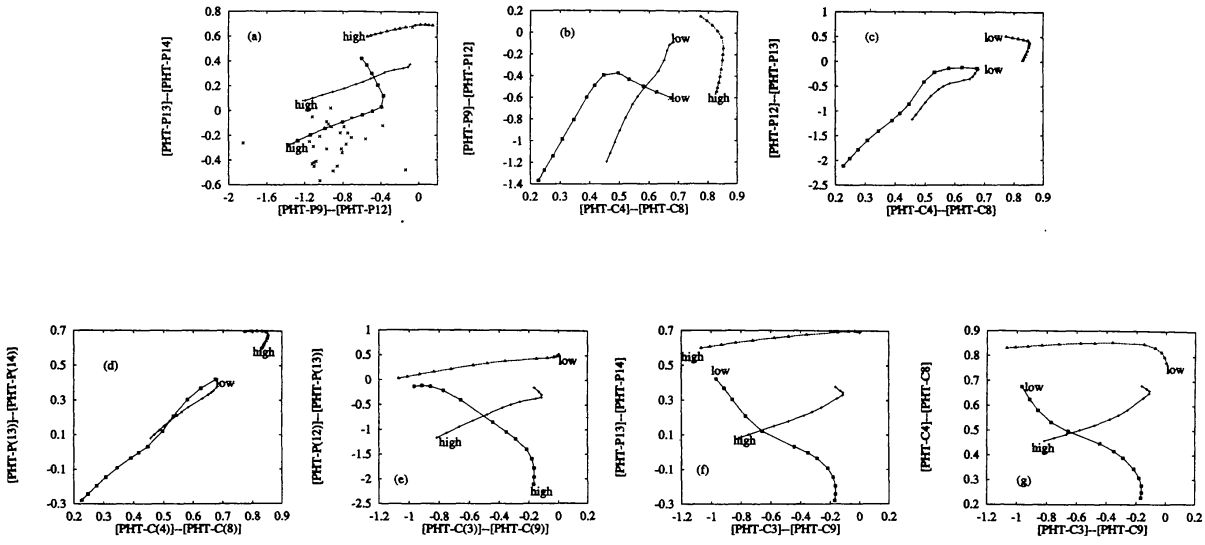

Figure 4. Colour-colour plots with O4 as the central star. The symbols □, + and Δ are for r^0, r^{-1} and r^{-2} density distributions respectively. "high" = higher τ_{100} and "low" = lower τ_{100} ends. × denote the datapoints from Crawford & Rowan - Robinson (1986).

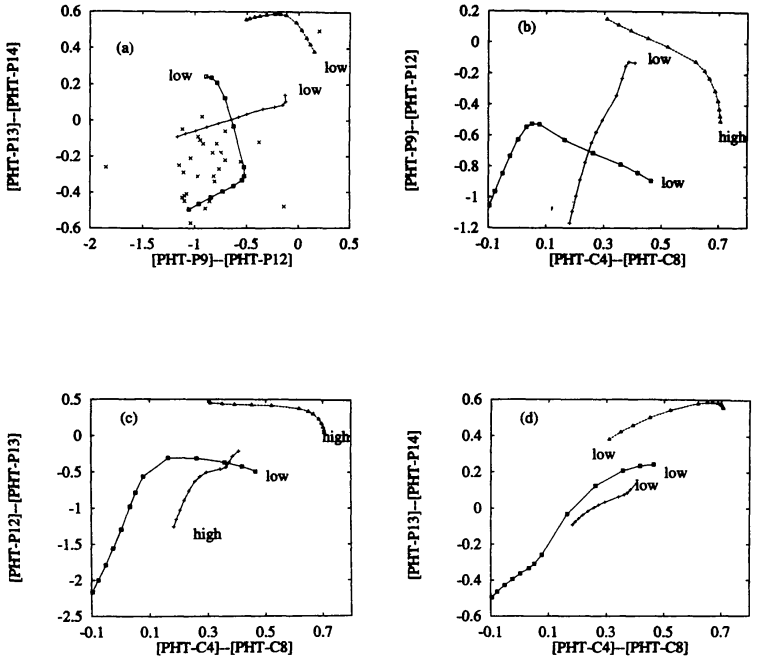

Figure 5. Colour-colour plots with O7 as the central star. The symbols □, + and Δ are for r^0, r^{-1} and r^{-2} density distributions respectively. "high" = higher τ_{100} and "low" = lower τ_{100} ends. × denote the datapoints from Crawford & Rowan - Robinson (1986).

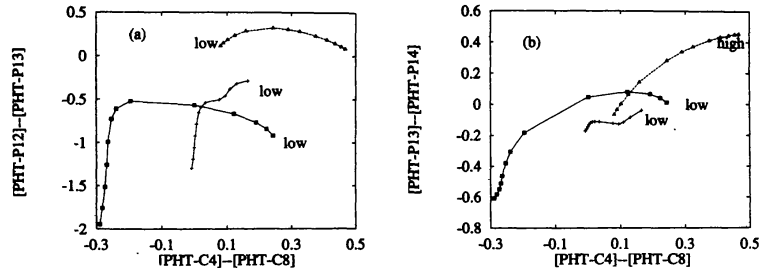

Figure 6. Colour-colour plots with B0.5 as the central star. The symbols □, + and Δ are for r^0, r^{-1} and r^{-2} density distributions respectively. "high" = higher τ_{100} and "low" = lower τ_{100} ends.

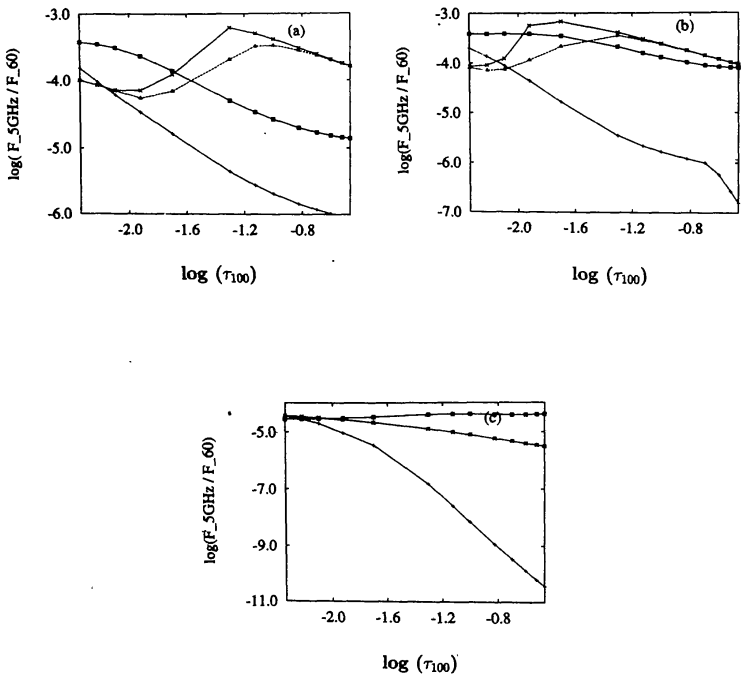

Figure 7. Plots of log of the ratio of radio flux density (F_{5GHz}) at 5GHz to the FIR flux density ($F_{60\mu m}$) at 60 μm as a function of the total radial optical depth (τ_{100}). The central stars in these models are : - O4 in (a), O7 in (b) and B0.5 in (c). The symbols □ and + are for r^0 and r^{-1} density distributions respectively and the symbols Δ and × are for r^{-2} distribution with $r_* = (R_{min}/2)$ and with $r_* = (R_{min} / 10)$ respectively.

3.2 Spatial / structural information

With the motive of assessing the diagnostic power of the spatial / structural information, the half width at half maxima (HWHM) sizes for some of our models are computed for the selected ISOCAM SW and LW filters (Table 5 of Paper I). The choice of the filters have been made in such a way that the true continuum is sampled and the spectral features (say due to Polycyclic Aromatic Hydrocarbon, PAH, etc.) are avoided. In a manner similar to Paper I, the wavelength dependence of these HWHM sizes have been fitted by a power law of the form $\theta_{1/2}(\lambda) = b \times \lambda^a$. The best fit values of '*a*' and '*b*' are listed in Table 4 for the selected models. The usefulness of the values of '*a*' & '*b*' are discussed in section 4.5.

3.3 Line emission from the gas

The line intensities emerging from the gas component of the model clouds, from various elements in their different ionization stages are subjected to the 'detectability' criteria of ISO spectrometers ISO-SWS and ISO-LWS. The detectability basically depends on the strength of

the line vis-a-vis neighbouring continuum emitted by the dust. This is quantified by the ratio of the powers falling on the relevant spectrometer resolution elements due to the line (P_{line}) and its neighbouring continua on both sides (P^{+}_{cont} & P^{-}_{cont}). We define the detectability parameter, $D=\log(P_{line} / \sqrt{P^{+}_{cont} \times P^{-}_{cont}})$, which is a measure of the line to continuum ratio. The spectral resolution, which is a function of the wavelength, ranges between 1000 – 20000 (de Graauw et al. 1996, Swinyard et al. 1996). In the present study, only those well detectable lines have been considered for which D > – 1.00, which is a rather conservative criterion.

Line emission within the wavelength range covered by the ISO spectrometers (2.5 μm – 200 μm) is considered here. The entire optical depth range is represented by three values which include the two extreme ones (τ_{100} = 0.0045 & 0.34). All the three density distribution laws (r^0, r^{-1} and r^{-2}) have been considered for all three types of exciting ZAMS stars. It was found from the CLOUDY runs that a superset of 27 lines describe the emission line spectrum for all the above models. These are listed in Table 5. However, this number drops to about half (for the lowest optical depth and constant density model) after the ISO detectability criterion is applied. A compact summary of the predicted emergent line luminosities and the line to continuum ratios are presented in Table 6, for all three types of the embedded stars, but only for the case of uniform density distribution and the lowest optical depth case. However, to demonstrate the role played by (a) the optical depth and (b) the radial density distribution law, on the emergent spectrum, results from selected models are shown in Figures 8-10 for the cases of exciting stars of type O4, O7 and B0.5 respectively. At the bottom of these figures, the positions of a few prominent fine structure lines, which are important coolants for the gas, are marked.

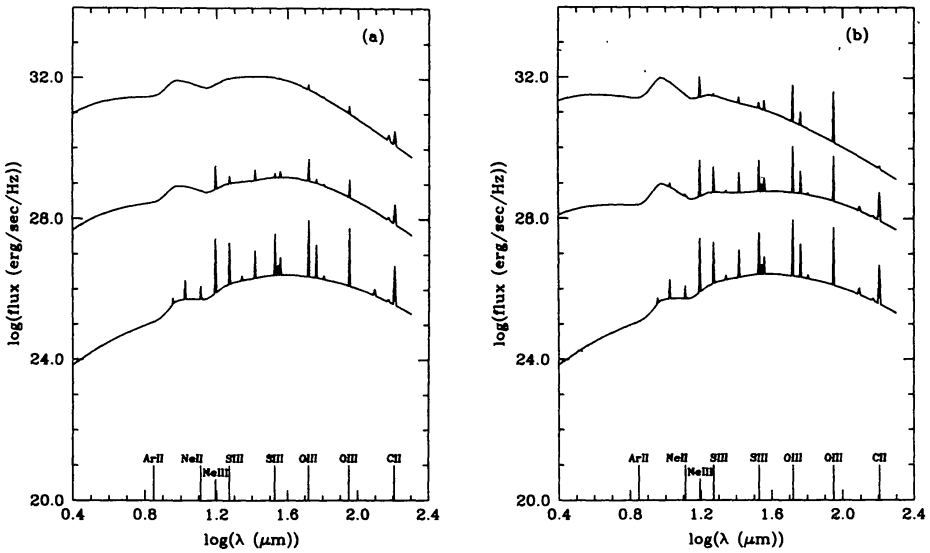

Figure 8. The emergent spectra from a spherical interstellar cloud with an embedded ZAMS star of O4 type. The wavelengths for a few prominent fine structure lines are marked near the abscissae. (a) The spectra for the case of uniform radial density distribution (r^0), and demonstrate the role of the optical depth. The three spectra correspond to the values of τ_{100} to be (i) 0.0045 (bottom), (ii) 0.075 (middle) and (iii) 0.34 (top). The curves (ii) & (iii) have been shifted by +3.0 (dex) & +6.0 (dex) respectively for clarity. (b) The spectra correspond to the case of τ_{100} = 0.0045, and show the effect of different radial density distributions. The three spectra refer to cases of (i) r^0 (bottom), (ii) r^{-1} (middle) & (iii) r^{-2} (top). The curves (ii) & (iii) have been shifted by +3.0 (dex) & +6.0 (dex) respectively for clarity.

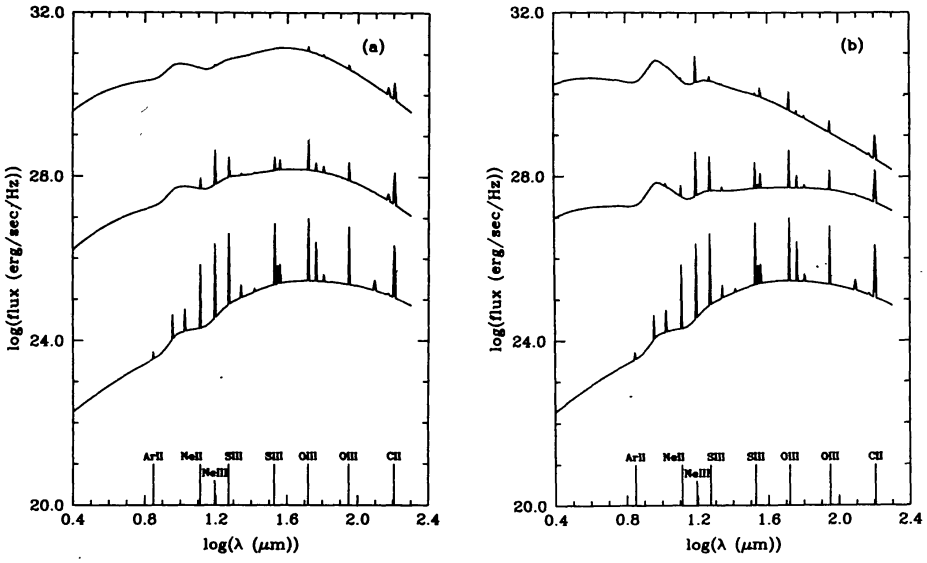

Figure 9. Same as in Figure 8, but for the case of a ZAMS star of O7 type embedded in the cloud.

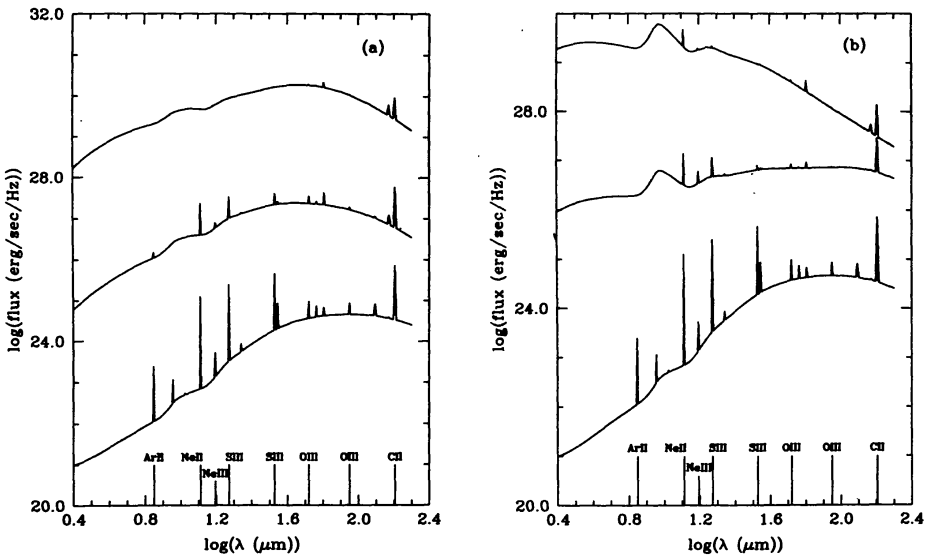

Figure 10. Same as in Figure 8, but for the case of a ZAMS star of B0.5 type embedded in the cloud.

4. Discussion

This study is aimed at identifying obserables, which are crucial to understanding some very basic parameters of compact H II regions. These parameters include the type of embedded star, temperature and density distribution in the cloud, elemental abundances, optical depth due to the dust etc. In this study, since the outer physical sizes are consistently frozen for all models, these are helpful in analysing compact H II regions, for which observational data regarding the physical sizes, hence distance and luminosity are known. These models would certainly help in identifying the region of the spectrum or the spectral lines, which bear most unique signature about the stellar type, as well as the dust density distribution.

An extremely conservative approach (as described in Paper I) is taken to decide which part of the continuum spectra is useful. Similar discretion is exercised, while choosing the spectral lines, for which the luminosities are presented here.

4.1 Mid infrared colours (PHT-P)

The mid-IR colour [P3-9] (Figure 1a) is measurable only if the exciting star is of type O4. Except for a small range of τ_{100} (0.06 – 0.04), the constant density case can be easily distinguished from other density distributions. The r^{-1} or r^{-2} cases can be separated for higher τ_{100} (> 0.1) cases. The colour [P9-12] (Figures 1b, 2a) is measurable for O4 and O7 type stars. The dust density distribution of r^{-2} can easily be distinguished from the other distributions using this colour. The difference between r^0 and r^{-1} can also be found for $\tau_{100} < 0.02$. To distinguish between the exciting stellar type, a very accurate measurement of this colour (< 0.005 dex) is required. The colour [P12-13] (Figures 1c, 2b, 3a) is measurable for all three types of exciting stars. Once again this colour can easily discriminate r^{-2} dust distribution law vis-a-vis r^0 or r^{-1} for all three types of exciting stars. For the stellar types O4 and O7, the cases r^0 and r^{-1} can be easily distinguished for $\tau_{100} > 0.03$, but requires better colour measurement for lower τ_{100} values. For B0.5 type star, the same can be done for any value of τ_{100} (except for a narrow region around 0.04) even with moderate accuracy of this colour. The colour [P13-14] (Figures 1d, 2c, 3b) with even moderate accuracy (0.005 - 0.1 dex), is extremely useful in distinguishing all the three density distribuions for both O4 and O7 type of exciting stars. However, for B0.5 type star, only for $\tau_{100} > 0.01$, this discrimination is possible. The distinction between the spectral type of the exciting star is possible for most of the τ_{100} range if the colour is available with good accuracy (<0.01 dex).

4.2 Far infrared colours (PHT-C)

The FIR colour [C4-8] (Figures 1e, 2d, 3c) can distinguish all three geometries for all three types of stars for $\tau_{100} > 0.01$. In addition, O4 can be easily distinguished from the other two star types. To identify between O7 and B0.5, the colour needs to be measured rather accurately (< 0.05 dex). The colour [C8-11] (Figures 1f, 2e, 3d) is very insensitive to the details of the models. If the colour is measured with better than 0.02 dex accuracy, then either the density distribution or the stellar type can be inferred.

4.3 Colour colour plots (CCP)

In case the far infrared optical depth is hard to estimate (no distance; no mass estimate from sub-millimetre flux density etc.,), then colour colour plot, CCP, is the only possible diagnostic tool available. A CCP is the locus of colour colour point as a function of τ_{100} in that plane. After studying several combinations of the colour colour plots, the most promising (i.e. with maximum diagnostic power of discriminating either the density distribution law and / or the embedded stellar type) are presented here. As a conservative practical criterion, only those CCPs are considered here, which change each colour by at least 0.7 dex over the entire τ_{100} range (0.0045 - 0.34) considered here. The number of CCPs with good diagnostic value reduce as the stellar type changes from O4 to O7 to B0.5.

4.3.1 Stellar type O4

A total of seven CCPs viz., [P13-14]/[P9-12], [P9-12/[C4-8], [P12-13]/[C4-8], [P13-14]/[C4-8], [P12-13]/[C3-9], [P13-14]/[C3-9] and [C4-8]/[C3-9] are presented in Figure 4. All these CCPs very clearly distinguish the r^{-2} density distribution law from the other two (r^0 and r^{-1}) for the entire range of optical depth considered in the present study. Of these, the first six (Figures 4(a)-(f)) can also distinguish between r^0 and r^{-1} density distributions with very moderate accuracies in colour determinations. The CCP [P13-14]/[P9-12} uses wavelength bands very close to those of IRAS mission. Hence, it is possible to compare existing measurements of compact H II regions with the model predictions. A sample of 27 compact H II regions selected by Crawford & Rowan-Robinson (1986), has been displayed on the plot for our models (Figure 4a). If the exciting stars for all these were O4, then the location of the observed points indicate density distributions and optical depths for these sources. Of 27, only one point falls on the r^{-2} curve and all the rest are scattered around the line corresponding to r^0 dust density distribution and spanning a τ_{100} range of 0.1 to 0.3. This result of predominance of uniform density distribution is consistent with the results of Faison et al. (1998), Campbell et al. (1995) & Mookerjea et al. (1999).

4.3.2. Stellar type O7

The four CCPs for the O7 case, viz. [P13-14]/[P9-12], [P9-12]/[C4-8], [P12-13]/[C4-8] and [P13-14]/[C4-8] are displayed in Figure 5. These CCPs have been found to be sensitive enough to be used as diagnostic tools. Among these CCPs the most sensitive one is the CCP [P12-13]/[C4-8] which distinguishes all the three density distributions even if the colours are measured with a very crude accuracy of 0.5 dex in [P12-13] and 0.2 dex in [C4-8]. For the rest, it is required to achieve a colour accuracy of < 0.1 dex to draw firm conclusions about density distribution and τ_{100}. Once again the r^{-2} law is the most unambiguously placed in all these CCPs. The IRAS measurements of the Carwford & Rowan-Robinson (1986) sample, have been overplotted on the CCP [P13-14] [P9-12] (Figure 5a). With the exception of one point close to the r^{-2} locus, most of the points are scattered between the loci corresponding to r^0 and r^{-1} density distributions. A comparsion of this CCP for O7 (Figure 5a) with that of O4 (Figure 4a) suggest that O7 is a better description of the observations. If the distances to the individual IRAS sources would be available, then on luminosity grounds, this conclusion could be

strengthened further.

4.3.3. Stellar type B0.5

Only two CCPs viz., [P12-13]/[C4-8] and [P13-14]/[C4-8], for the B0.5 type case (Figure 6) were found to be sensitive enough for extracting source details. Like the earlier case of O7, the CCP [P12-13]/[C4-8] is very sensitive and can distinguish density distribution laws from a crude [P12-13] colour and a moderate accuracy [C4-8]. The CCP [P13-14]/[C4-8] is the unique example among all CCPs for all exciting stars where the locus for r^{-2} density distribution intersects the r^0 case.

4.4 Radio continuum to FIR ratio

For the calculation of the radio continuum, following scheme I, the inner radius for the gas cloud is assumed to be 0 for r^0 and r^{-1} distributions. This practical assumption is physically equivalent to the gas shell starting very close to the stellar surface. However, the same is not mathematically possible for an r^{-2} distribution, hence the inner gas radius has been chosen to have a non-zero r_*. Two values of r_* have been considered, viz., 10% and 50% of the radius of the cavity in the dust cloud and the effect of these assumptions are presented in Figure 7. It is apparent that the choice of r_* causes difference in the ratio, $F_{5GHz}/F_{60\mu m}$, for some intermediate values of τ_{100}, for O4 and O7 stars and has no effect when the exciting star is of type B0.5.

For the case of O4, all three density distributions can be identified at any value of τ_{100}. For the rest, this capability exists only for $\tau_{100} > 0.05$. In general, for r^{-1} case the radio to FIR flux density ratios is most sensitive to τ_{100}. At higher optical depths, this ratio can easily distinguish between the three types of exciting stars for any geometry.

4.5 Structural information

From a careful study of Table 4, the following comments can be made regarding the diagnostic value of the structural parameters '*a*' and '*b*'. The parameter '*b*' is extremely sensitive to the spectral type of the embedded star, for a wide range of τ_{100} as well as the three density distributions (r^0, r^{-1} & r^{-2}). The parameter '*a*' is reasonably sensitive to the dust optical depth and can also distinguish between the constant density distribution from the rest.

So, in conclusion, the structure parameters have good diagnostic value for identifying type of embedded source and the optical depth, but regarding density distribution they can distinguish only between the r^0 case from the rest (r^{-1} & r^{-2}).

4.6 Information from the line emission

The diagnostic value of the fine structure lines have been quantified in terms of lines detectable above the continuum, for the spectrometers ISO-LWS and ISO-SWS, for realistic instrumental resolution. The number of detectable lines depends on the type of exciting star, the radial density profile and the absolute values for the densities of the gas and the dust, with relative

abundance of elements being the same for all models. In general, the number of detectable lines (D > –1.00) reduces as one goes from O4 to O7 to B0.5, as the luminosity and effective temperature of the embedded star reduces. Also for the r^0 case, the detectable lines are more numerous than r^{-1} case. Similarly r^{-1} case has more lines than the r^{-2} case in general.

In addition to the absolute luminosities of these lines, it is important to know the line to continuum contrast, the parameter D, which identified lines that are more easily detectable. The values of D are also listed in Table 6, along with the line luminosities, for the selected models.

Table 6. The line luminosity (L) and detectability (D) parameters for the case of constant density distribuion (r^0) and $\tau_{1(0)}$ = 0.0045. The results correspond to the embedded ZAMS stars of spectral type O4, O7 and B0.5.

Lines	λ	O4		O7		B0.5	
	μm	L (erg/sec)	D	L (erg/sec)	D	L (erg/sec)	D
C II	157.7	1.22(35)	1.05	5.58(34)	1.23	1.94(34)	1.30
O I	145.6	2.46(33)	–0.77	4.58(32)	–0.95	--	--
N I	121.8	1.36(34)	–0.28	4.63(33)	–0.13	1.41(33)	–0.04
O III	88.4	2.74(36)	1.62	2.88(35)	1.38	1.97(33)	–0.07
O I	63.2	3.25(34)	–0.56	7.73(33)	–0.32	1.52(33)	–0.21
N III	57.2	1.06(36)	0.87	1.45(35)	0.89	2.17(33)	–0.08
O III	51.8	6.37(36)	1.57	6.64(35)	1.51	4.27(33)	0.21
Ne III	36.0	2.34(35)	0.32	1.93(34)	0.27	--	--
Si II	34.8	9.78(34)	–0.06	1.83(34)	0.25	2.78(33)	0.50
S III	33.5	1.59(36)	1.14	3.16(35)	1.48	1.98(34)	1.37
O IV	25.9	6.15(35)	0.70	1.93(33)	–0.66	--	--
Ar III	21.8	4.49(34)	–0.44	7.79(33)	0.02	2.08(32)	–0.26
S III	18.7	1.59(36)	1.14	3.17(35)	1.72	1.96(34)	1.87
Ne III	15.6	2.55(36)	1.54	2.14(35)	1.81	3.71(32)	0.46
Ar V	13.1	8.06(33)	–0.87	--	--	--	--
Ne II	12.8	8.09(34)	0.11	8.05(34)	1.53	1.45(34)	2.25
S IV	10.5	3.73(36)	0.40	1.14(35)	0.38	--	--
Ar III	8.99	5.97(35)	–0.30	1.05(35)	0.48	2.79(33)	0.44
Ar II	6.99	--	--	--	--	1.00(34)	1.31

We note that for O4 star and r^0 density distribution (Table 6), the [O III] (51.8 μm) line happens to be the most luminous. However, from the viewpoint of the line to continuum ratio, for the same family of models, the [O III] (88.4 μm) line is found to have the best detectability . This suggest that while the absolute luminosity of the lines are helpful for understanding the different physical parameters, the relative contrast of the lines with respect to the local continuum bear useful information about the actual appearance of the spectrum and hence the detectability of a particular line. The latter is extremely useful from the observation point of view. Based on the results presented here (Table 6 & Figs. 8 -10), many quantitative inferences can be drawn, like the following : (i) exact luminosity as well as detectability (for the ISO spectrometers) sequence of spectral lines; (ii) role of a particular line in cooling of the interstellar medium (ISM) near H II regions; (iii) relative roles of different elements in the energetic of the ISM; (iv) expected line ratios for the same species (being abundance independent) under different

physical conditions in / near H II regions, as a function of optical depth & density distribution; (v) the role of the continuum from the dust, in highlighting or suppressing expected detection of various fine structure lines; etc.

From the above it is very clear that the details of optical depth, the exciting stellar type (luminosity and effective temperature) as well as the dust density distribution are well imprinted on the emergent line spectrum of the compact H II region. Hence, the present study has quantitatively demonstrated the diagnostic value of several fine structure lines of abundant elements in the interstellar medium. The same can be used extensively in studies dealing with ISO spectrometer in near future.

Within the published ISO-SWS spectra, though with limited wavelength coverage of compact H II regions (Roelfsema et al. 1996) we notice that one of their sources viz., IRAS 21190+5140, approximately matches our prediction for a O7 star embedded in a uniform density of total radial $\tau_{100\mu m} = 0.0045$. Not only the two line luminosities at 8.99 μm [Ar III] and 10.5 μm [SIV], but also the nearby continuum are roughly matching the predictions. This is only to indicate the usefulness of the present results. Obviously a finer tuning of the parameters near these values would be needed before firm conclusions can be drawn about this source.

5. Summary

The present work is a generalized extension of an earlier study (Paper I) of infrared diagnostics for compact H II regions by including spectroscopic tools (in addition to the earlier approach using the photometric & imaging information). Self-consistent radiation transfer (in spherical geometry) through the interstellar cloud, has been carried out to predict emergent spectrum originating from both the dust as well as the gas components. This also includes detailed predictions about the infrared fine structure line emission of several heavy elements (in different ionization stages). The effects of different exciting stars (O4, O7 and B0.5) and different radial profiles (r^0, r^{-1} and r^{-2}) of densities have been explored. All the models studied here correspond to a fixed outer physical dimension.

Diagnostically, the most useful (photometric as well as spectroscopic) information of the emergent spectrum from the compact H II regions, have been quantitatively identified. For ease of comparison, the model predictions have been expressed in terms of directly observable quantities through the instruments onboard ISO. The predictions about the continuum are expressed in terms of colours and the spectral line results are expressed as luminosities and line to local continuum constraints (detectability).

The density distribution is well understood, by some of the colours presented here. In the absence of any information regarding the optical depth of the H II region, the colour-colour plots presented here, provide useful information about the spectral type of the embedded star as well. The ratio of the radio continuum to the FIR flux density, found to be the most sensitive to τ_{100} for r^{-1} distribution, contains useful information about the stellar type and also density distribution of the H II regions. The angular sizes are also diagnostically very important. The luminosity of fine structure lines are shown to be extremely rich in information about the geometric and physical details of the H II regions.

The results of the present study and the Paper I, would be extremely useful, for statistical studies on huge sample of data, from the space mission ISO, expected to be publicly available in the near future. It also presents a very general method of modelling, which can be used very efficiently for individual compact H II regions.

Acknowledgements

It is a pleasure to thank D. Narasimha for many useful discussions.

References

Baldwin J., Ferland G. J., Martin P. G., et al., 1991, ApJ, 374,580.

Clegg E., Ade P. A. R., Armand C. et al., 1996, A&A, 315, L38.

Crawford J., Rowan - Robinson M., 1986, MNRAS, 221, 923.

de Graauw Th., Haser L. N., Beintema D. A. et al., 1996, A & A, 315, L49.

Egan M. P., Leung C. M., Spagna G. F., 1988, Computer Physics Communications, 48, 271.

Elitzur M., 1982, Review of Modern Physics, 54, 1125.

Faison M., Churchwell E., Hofner P. et al., 1998, ApJ, 500, 280.

Ferland G. J., 1996, *Hazy*, a Brief Introduction to CLOUDY, Univ. of Kentucky, Dept. of Phys. and Astron. Internal Reports.

Keto E. R., 1990, ApJ, 355, 190.

Mookerjea B., Ghosh S. K., Karnik A. D., Rengarajan T. N., Tandon S. N., & Verma R. P., 1999, ApJ, 522, 285.

Mookerjea B., Ghosh S. K., 1999a, BASI, 27, 585, (Paper I), .

Mookerjea B., Ghosh S. K., 1999b, J. Astrophys. Astr., 20, in press.

Olmi L., Cesaroni R., Walmsley C. M., 1995, BAAS, 36.01, 186.

Osterbrock D. E., Tran H. D., Veilluex S., 1992, ApJ, 389, 305.

Roelfsema P. R., Cox P., Tielens A. G. G. M et al., 1996, A&A, 315, L289.

Rubin R. H., Simpson J. R., Haas M. R., Erickson E. F., 1991, ApJ, 374, 564.

Swinyard B. M., Clegg P. E., Ade P.A.R., 1996, A&A, 315, L43.